Asteroids, second part.
Summary

- Reflection of light from the surface of asteroids and its relation to meteorites.
- Taxonomy of asteroids (asteroid classes) based on reflectance spectra.
- Spatial distribution of asteroid classes in the main belt.
- Thermal models of asteroids including heat transport.
- Yarkovsky effect of non-gravitational motion of small asteroidal bodies.
- Size distribution and collisional evolution of asteroids – zodiacal bands.
- Asteroid rotation
- Cratering by impacts
- Sizes and densities of asteroids
- Asteroids imaged by spacecraft: Gaspra, Ida with moon Daktyl, Matilda, Eros
- Space weathering

Asteroid surface mineralogy
a: nickel-iron metal
b: olivine
c: orthopyroxene
d: plagioclase feldspar
e: spinel-bearing Allende inclusion

Note:
Olivine: SiO_4 anion of finite size.
Pyroxene SiO_3 anion of "infinite" size, forming bands or leaves.
In both cases the metals like Fe are responsible for the spectral signature.

Gaffey et al. Asteroids II, Binzel et al. eds., U. of Arizona press, Tucson 1989, pp 98-127.

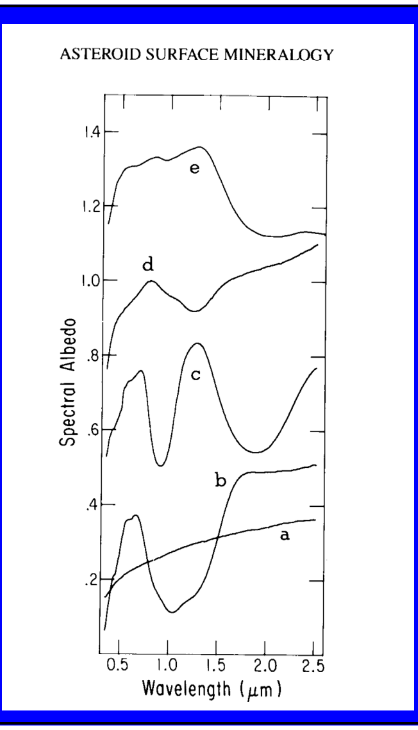

Crystalline structure

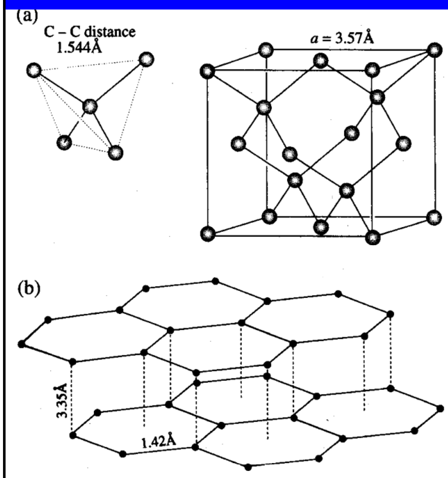

FIGURE 5.2 (a) Mineral structure of diamond: each carbon atom is surrounded by four others in a regular tetrahedron (shown by the dashed line, left figure). The diamond (right figure) is built up from these tetrahedra. (Putnis 1992) (b) The structure of graphite is made up of layers in which the carbon atoms lie at the corners of a hexagonal mesh. Within the layers the atoms are strongly bonded, while the layers are weakly bonded to each other. (Putnis 1992)

Chemical composition

TABLE 5.2 Chemical Classes of Minerals[a].

Class	Defining anions	Example
Native elements	none	Copper Cu, gold Au
Sulfides and similar compounds	S^{2-} similar anions	Pyrite FeS_2
Oxides and hydroxides	O^{2-} OH^-	Hematite Fe_2O_3 Brucite $Mg(OH)_2$
Halides	Cl^-, F^-, Br^-, I^-	Halite NaCl
Carbonates and similar compounds	CO_3^{2-}	Calcite $CaCO_3$
Sulfates and similar compounds	SO_4^{2-} similar anions	Barite $BaSO_4$
Phosphates and similar compounds	PO_4^{3-} similar anions	Apatite $Ca_5F(PO_4)_3$
Silicates and similar compounds	SiO_4^{4-}	Pyroxene $MgSiO_3$

[a] After Press and Siever (1986).

Abundant minerals, (DePater/Lissauer Planetary Sciences, p. 138ff)

Minerals are characterized by chemical compostion and crystalline structure (example: diamond and graphite)
Silicates: Quarz (SiO_4), olivine (Fe,Mg)2SiO_4 (heaviest of silicates); feldspar , 60% on Earth, (K,Na)$AlSi_3O_8$, $CaAl_2Si_2O_8$, orthoclase (K-rich), plagioclase (Na and/or Ca rich); pyroxenes (10%, heavier than feldspars), augite (Ca(MgFeAl)$(AlSi)_2O_6$), enstatite ($MgSiO_3$), hypersthene (Mg,Fe)SiO_3; amphiboles (Mg,Fe,Ca)-silicates, slightly less dense than pyroxenes and more amorphous, e.g. hornblende.
Oxides: magnetite (Fe_3O_4), hematite (Fe_2O_3), limonite ($HFeO_2$), ilmenite ((Fe,Mg)TiO_3), perovskite ($CaTiO_3$), spinel ($MgAl_2O_4$)

Hydrated minerals

Phyllosilicates (clay minerals): different numbers of OH groups between the two silicate layers, serpentine, mostly in carbonaceous meteorites, 3µm ice feature, 0.7µm dip.
Such minerals are typical for so-called C-type “carbonaceous” objects.

Rocks

primitive rocks, igneous rocks, metamorphic rocks, sedimentary rocks, breccias

basalt (MgFe) mafic rock, ultramafic rocks (heavy elements)
feldspar (orthoclase) and quarz form granite

Note: in asteroids (and meterorites) there is a surprisingly large number of igneous rocks.

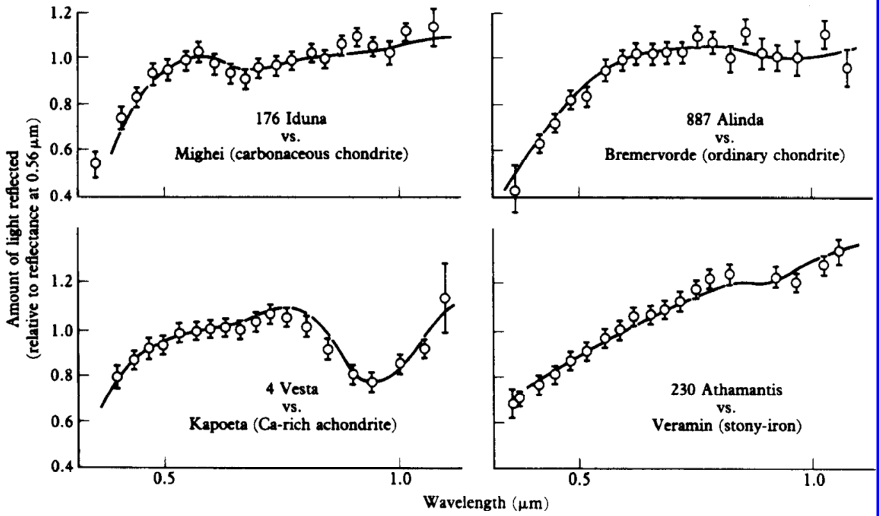

FIGURE 8.8 A comparison of the reflection spectra of four asteroids (points with error bars) with meteorite spectra as determined in the laboratory. (Morrison and Owen 1996)

Morrison and Owen 1996, The planetary system, Addison-Wesley, New York.

Note absorption dip at 0.7μm in 176 Iduna, characteristic of hydrated minerals

Asteroid reflectance spectra:

Left panel: 1 Ceres (C), 4 Vesta (V), 44 Nysa (E), 349 Dembovska (R)

Right panel: 8 Flora (S), 15 Eunomia (S), 16 Psyche (M), 113 Amalthea (S, offset by +0.1), 354 Eleonora (S, offset by +0.1), and 446 Aetarnitas (A, offset by 0.2) (Gaffey et al. 1989, prev. slide)

Far right panel: Spectra of 2060 Chiron (top), 944 Hidalgo (middle), and 5145 Pholus (bottom)

(Luu J.X., Icarus 104, 138-148, 1993)

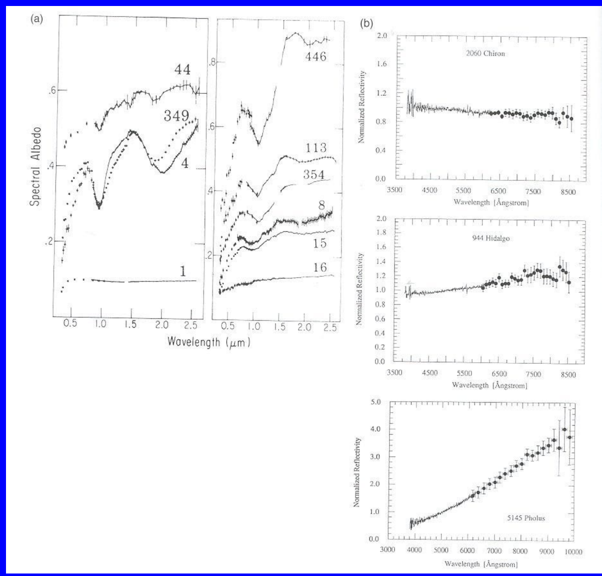

TABLE 9.4 Asteroid Taxonomic Types.	
Low-albedo classes:	
C	Carbonaceous asteroids; similar in surface composition to CI and CM meteorites. Dominant in outer belt beyond 2.7 AU. UV absorption feature shortwards of 0.4 μm. Spectrum flat, slightly reddish longwards of 0.4 μm. Subclasses: B, F, G.
D	Red featureless spectrum, possible due to organic material. Extreme outer belt and Trojans.
P	Spectrum is flat to slightly reddish; shape resembles that of M type asteroids. Outer and extreme outer belt.
K	Resembles CV and CO meteorites.
T	Moderate absorption feature shortwards of 0.85 μm; flat spectrum at longer wavelengths. Rare, unknown composition. Possibley highly altered C types

Moderate-albedo classes:	
S	Stony asteroids. Major class in inner to central belt. Absorption feature shortward of 0.7 µm. Weak absorption bands near 1 and 2 µm.
M	Stony-iron or iron asteroids; featureless flat to reddish spectrum.
Q	Resembles ordinary (H, L, LL) chondric meteorites. Absorption features shortwards and longwards of 0.7 µm. 1862 Apollo is type example.
A	Very reddish spectrum shortwards of 0.7 µm. Strong absorption feature near 1 µm.
V	Strong absorption feature shortwards of 0.7 µm, and near 1 µm. Similar to basaltic achondrites. Type example: 4 Vesta
R	Spectrum intermediate between A and V classes. Similar to that of olivine-rich achondrites. Type example: 349 Dembowska.

High-albedo (> 0.3) class:	
E	Enstatite asteroids. Concentrated near inner edge of belt. Featureless, flat to slightly reddish spectrum.

Note: enstatite $Mg[SiO_3]$ is also a pyroxene.

(a) Graph showing the relative distribution of the asteroid taxonomic classes as a function of heliocentric distance. The classes E, S, C, M, P and D are shown. Smooth curves are drawn through the data points for clarity. (Gradie *et al.* 1989)

(b) Distribution of igneous, primitive and metamorphic classes as a function of heliocentric distance. (This figure assumes that S type asteroids are igneous bodies.) (Bell *et al.* 1989)

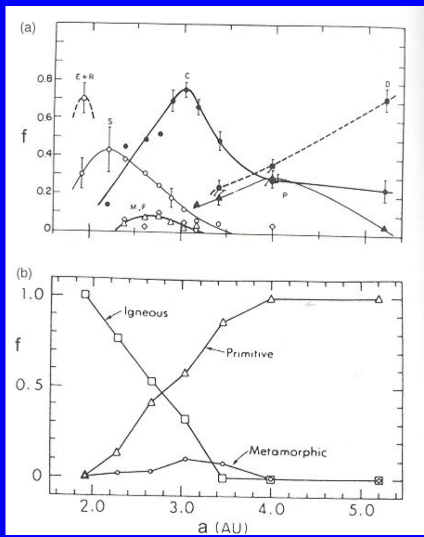

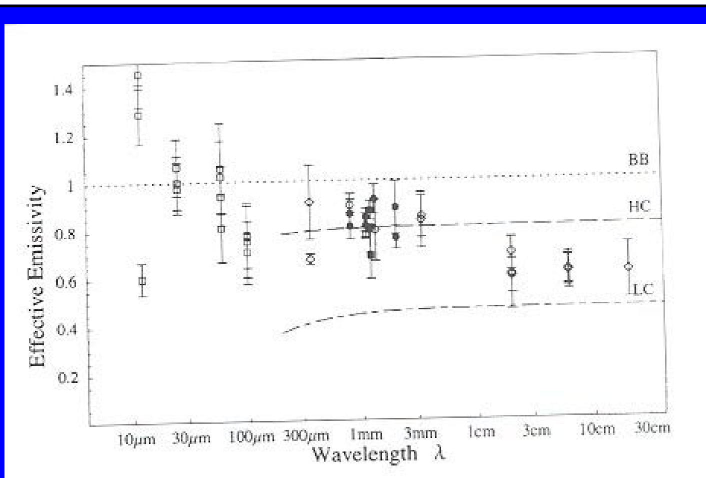

Microwave spectrum of 1 Ceres. The curves represent different models. BB is a black body model. Model HC is for a rapidly rotating sphere, overlain by material with a high thermal conductivity. LC is a model of low thermal conductivity (Redman *et al.* 1998)

Size distribution and collisional evolution

$N(R) = N_0 (R/R_0)^{-\zeta}$, for $R_{min} < R < R_{max}$
A population of collisionally evolving bodies will at the end arrive at a power law size distribution with $\zeta = 3.5$, provided the collision process is self-similar.
$\zeta = 3.5$ implies that most of the mass is in the largest body and most of the surface area in the smallest bodies.

Collisions:
V_{escape} from 1 Ceres = 0.6 km s-1. Thus, most collisions are erosive or disruptive.
Hirayama families with similar orbital elements *a, e, i.*
Dust bands.

The relative size distribution as observed for asteroids, with superposed lines which correspond to power law size distributions with $\zeta = 3$, and $\zeta = 4$ (Gradie et al. 1989).

$N(R) = N_0 (R/R_0)^{-\zeta}$

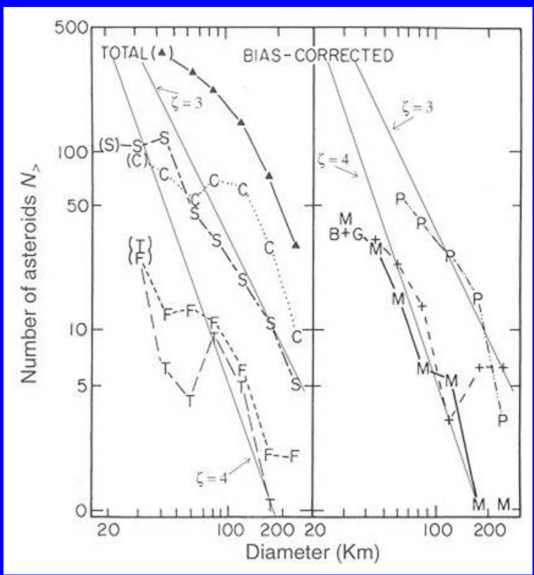

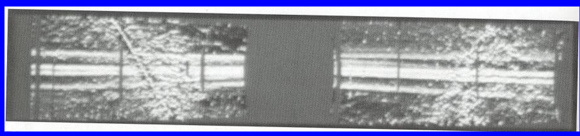

IRAS image at 25 μm of several zodiacal dust bands in the asteroid belt. Parallel bands are seen above and below the ecliptic, encircling the inner Solar System. The two central bands are connected to the Koronis-Themis families, and the 10° bands may be from the Eros family. The thin band between the center bands and the outer 10° bands is a type 2 dust trail. Type I dust trails originate from short-period comets; type 2 dust trails have not yet been understood. It could signify a relatively recent break-up of an asteroids. The diagonally shaped bands are the galaxy. (Courtesy: M.V. Sykes)

If a body is not completely shattered and the relative velocities are insufficiently large some of the fragments may coalesce back and form a rubble pile. Multiple asteroid systems may form in this way.

Multiple asteroid systems are tidally unstable, but nevertheless seem to be quite frequent. 243 Ida and Dactyl are an example. From 200 asteroids observed with an adaptive optics system 3 turned out to be double. Double impact craters exist on Earth (Clearwater lakes in US, Ries and Steinheimer Becken in Germany) and other planets. Dumbbell shaped asteroids.

(a) Histogram of the number of asteroids as a function of rotation rate (expressed in revolutions per day) for asteroids of various sizes. (Binzel *et al.* 1989)

(b) Rotation period (number of revolutions per day) as a function of asteroid diameter. (Binzel 1992)

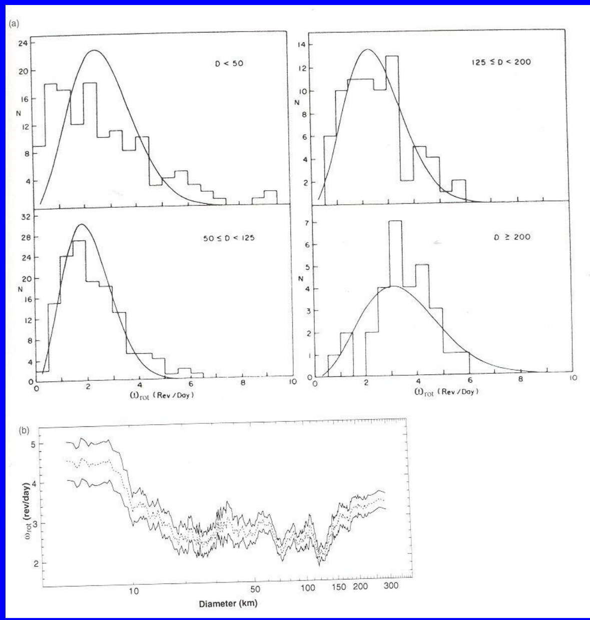

Impact craters

(a)

(b)

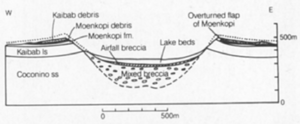

FIGURE 5.21 (a) Meteor crater in Arizona. The crater has a diameter of 1 km and is 200 m deep. (Courtesy: D. Roddy, USGS/NASA) (b) A cross-section through Meteor crater. (Melosh 1989, as derived from Shoemaker 1960)

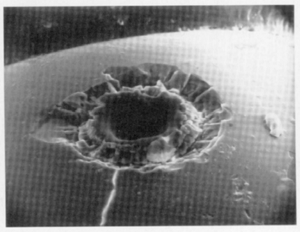

FIGURE 5.22 Microcrater or pit with a diameter of 30 μm. This is a scanning electron microprobe photograph of a glass sphere on the Moon, found by Apollo 11. (Courtesy: D. McKay,

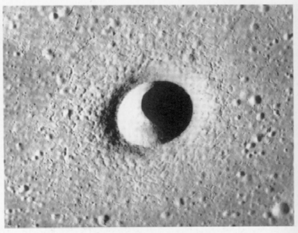

FIGURE 5.23 A small or simple crater: this is a photograph of the 2.5-km diameter crater Linné in western Mare Serenitatis on the Moon. (NASA/Apollo panoramic photo AS15-9353)

FIGURE 5.24 A close-up of the 75-km diameter complex lunar crater King, characterized by a relatively flat crater floor, a central peak and terraced walls. (NASA/Apollo Hasselblad photo AS16-122-19580)

Physics of an impact

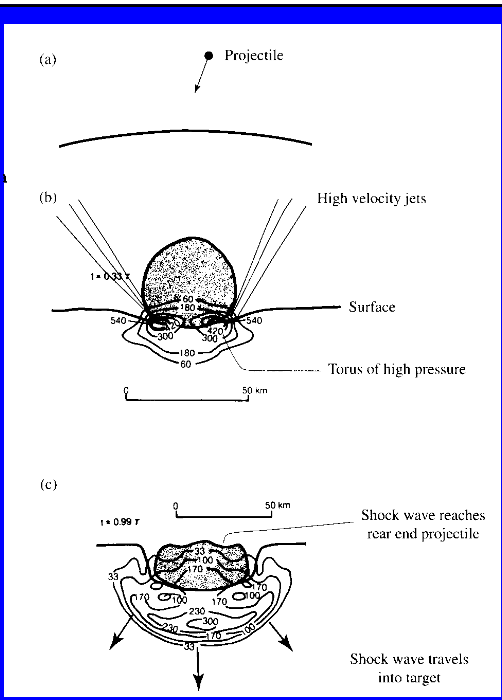

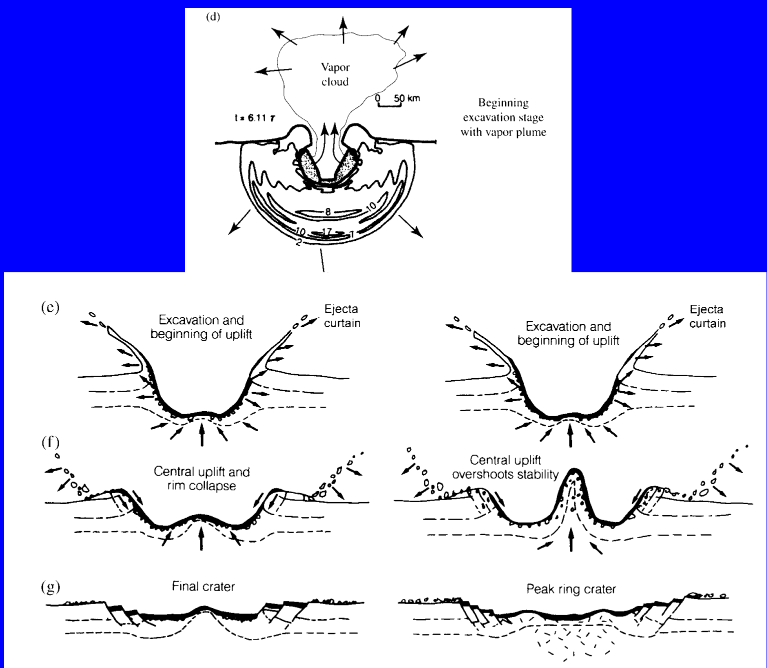

Ries (24 km diameter) and Steinheimer Becken (3.4 km diameter) are two impact craters, located a few km apart in southern Germany near the city of Nördlingen. They formed 14.8 million years ago. The picture shows the Steinheimer Becken. Note the central elevation.

Masses of asteroids

Masses of asteroids can be determined only from their gravitational action on other (preferably smaller) objects. In this way the masses of the asteroids of large size have been determined.

The masses of Ida and Mathilde have been determined from the orbital change of the Galileo or NEAR-Shoemaker spacecraft.

The mass of Eros is best known as the NEAR-Shoemaker spacecraft was an artefical satellite of Eros.

TABLE 9.3 Sizes and Densities of Asteroids and Martian Moons.

Body	Class	R (km)	ρ (g cm^{-3})	Ref.
1 Ceres	G	457	2.7 ± 0.14	1
2 Pallas	M	262	2.6 ± 0.5	1
4 Vesta	V	251	3.62 ± 0.35	2
10 Hygiea	C	215	2.05 ± 1	3
45 Eugenia	C	215	1.2	4
87 Sylvia	PC	135	1.6 ± 0.1	5
216 Kleopatra	M	$217 \times 94 \times 81$	>3.5	6
243 Ida	S	$28 \times 12 \times 7.4$	2.6 ± 0.5	7
253 Mathilde	C	$33 \times 24 \times 23$	1.3 ± 0.2	8
433 Eros	S	$31 \times 13 \times 13$	2.67 ± 0.03	9
762 Pulcova	C	140	1.8	10
1996 FG_3	C	1.4	1.4 ± 0.3	11
2000 DP_{107}	C	0.40	$1.6^{+0.7}_{-0.2}$	5
2000 UG_{11}	R	0.115		5
Phobos	C	$13.3 \times 11.1 \times 9.3$	1.9 ± 0.1	12
Deimos	C	$7.5 \times 6.1 \times 5.2$	1.8 ± 0.2	12

1: Millis *et al.* (1987). 2: Millis and Elliot (1979). 3: Scholl *et al.* (1987). 4: Merline *et al.* (1999). 5: Margot *et al.* (2000). 6: Ostro *et al.* (2000). 7: Thomas *et al.* (1996). 8: Veverka *et al.* (1997). 9: Yeomans *et al.* (2000). 10: Merline *et al.* (2000). 11: Mottola and Mahulla (2000), and Pravec *et al.* (2000). 12: Thomas (1999).

Non-gravitational forces on asteroids – the Yarkovsky effect.

There are several radiative effects affecting the motion of solid bodies in the solar system. For small particles like cometary particles the most important one is solar radiation pressure (see below in comet lecture). For cm-sized particles there is the Pointing-Robertson drag, caused by fact that the radiation of thermal emission, which is isotropic in the particle's rest frame is anisotropic in the rest frame of the Sun.

The Yakovsky effect is caused by the anisotropy of thermal radiation of a macroscopic body. Such an anisotropy may be caused by thermal inertia: the body is warmer on its afternoon side as compared to its morning side. For a mean temperature T and a temperature difference between morning and evening hemisphere of ΔT the transverse force F_y is given by

$$F_Y = \frac{8}{3}\pi R^2 \frac{\sigma T^4}{c} \frac{\Delta T}{T} \cos\psi,$$

R asteroid radius, σ Stefan-Boltzmann constant, and ψ the obliquity of the asteroid's pole, i.e. angle between rotation axis and ecliptic pole. This effect is e.g. important to transport meteorites from the asteroid to the Earth.

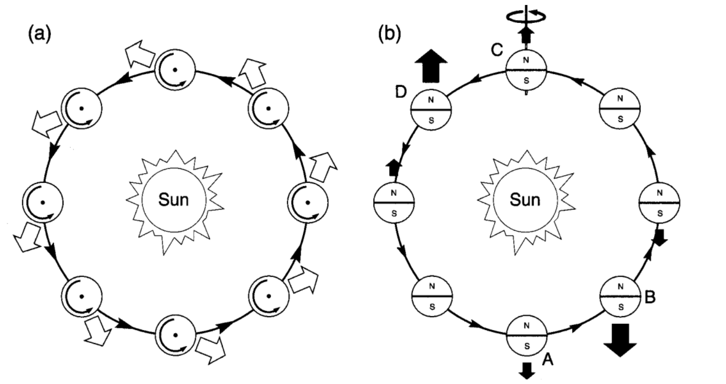

Fig. 1. **(a)** The diurnal Yarkovsky effect, with the asteroid's spin axis perpendicular to the orbital plane. A fraction of the solar insolation is absorbed only to later be radiated away, yielding a net thermal force in the direction of the wide arrows. Since thermal reradiation in this example is concentrated at about 2:00 p.m. on the spinning asteroid, the radiation recoil force is always oriented at about 2:00 a.m. Thus, the along-track component causes the object to spiral outward. Retrograde rotation would cause the orbit to spiral inward. **(b)** The seasonal Yarkovsky effect, with the asteroid's spin axis in the orbital plane. Seasonal heating and cooling of the "northern" and "southern" hemispheres give rise to a thermal force that lies along the spin axis. The strength of the reradiation force varies along the orbit as a result of thermal inertia; even though the maximum sunlight on each hemisphere occurs as A and C, the maximum resultant radiative forces are applied to the body at B and D. The net effect over one revolution always causes the object to spiral inward.

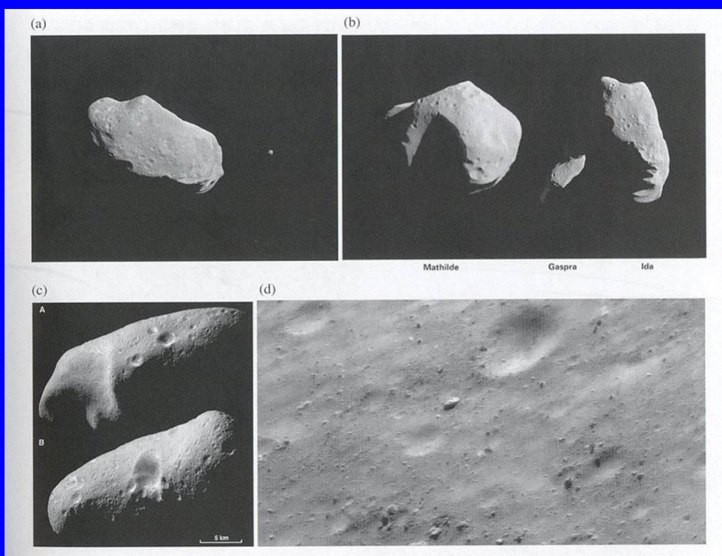

Keck adaptive optics image of 4 Vesta. Bright and darker bands are clearly visible. Image is taken at 2.1 µm. The resolution is 50 mas. (Courtesy: Keck Observatory Adaptive Optics Team)

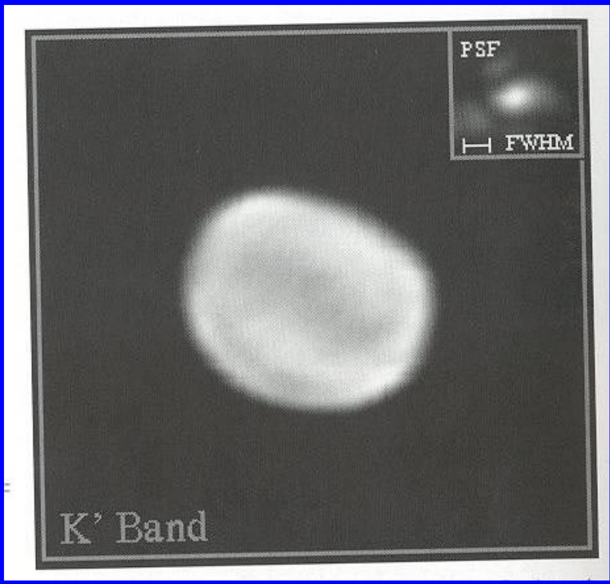

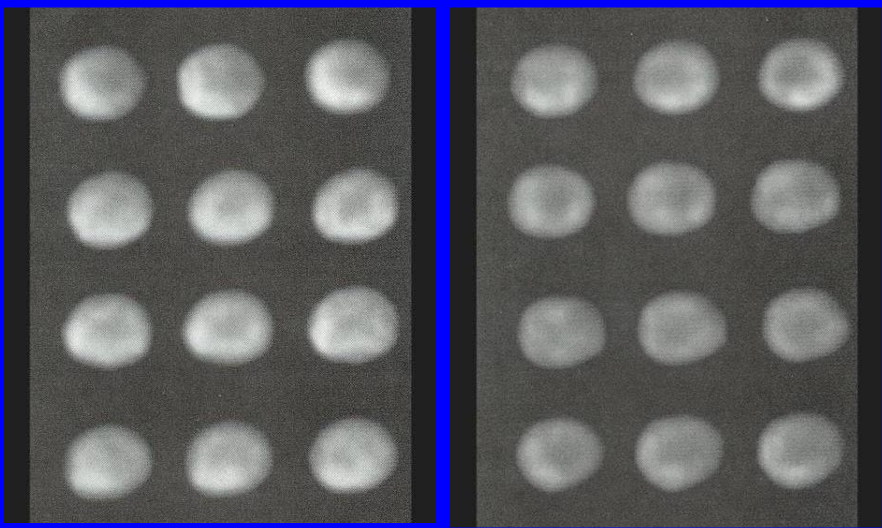

Maximum entropy restoration of Hubble Space Telescope WFPC2 images of Asteroid 4 Vesta in the red spectral region. One row = one image sequence with images taken 8 minutes apart. The eight rows cover one full rotation of Vesta. The solar phase angle was about 12° (Zellner et al., Icarus 128, 83, 1997).

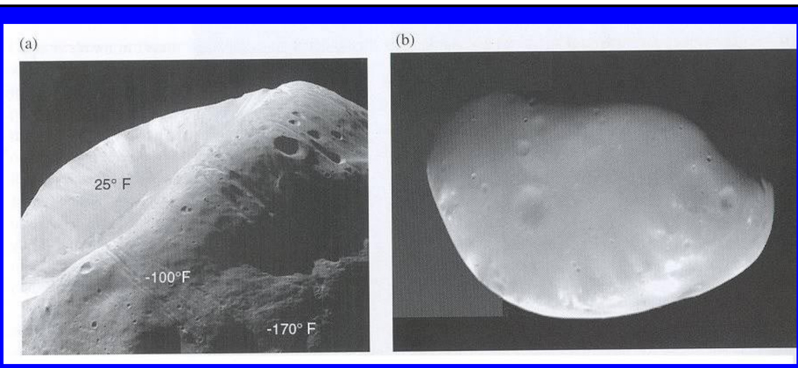

(a) Image of Phobos, the inner and larger of the two moons of Mars, taken by the Mars Global Surveyor in 1998. The Thermal Emission Spectrometer (TES) measured the brightness of thermal radiation at the same time the camera acquired this image. By analyzing the brightness, TES scientists could deduce the various fractions of the surface exposed to the Sun and their temperatures. This preliminary analysis shows that the surface temperature, dependent on slope and particle size, varies from a high of +25 °F (-4° C) on the most illuminated slopes to -170 °F (-112 °C) in shadows. This large difference, and the fact that such differences can be found in close proximity, adds support to the notion that the surface of Phobos is covered by very small particles. (NASA/Mars Gloval Surveyor PIA01332) (b) Viking image of the martian satellite Deimos.

The following asteroid images are from http://photojournal.dlr.de/

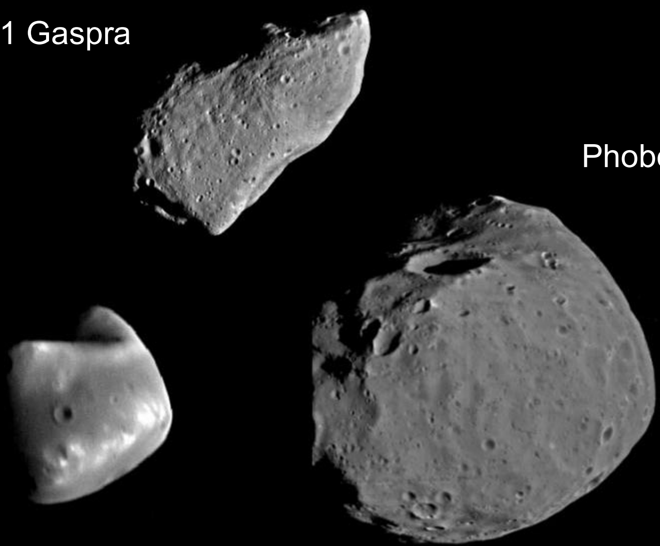

951 Gaspra, Oct. 29, 1991
Size 17 x 13 km
Spin period 7 hours.
Origin from comparatively recent collisional break-up of a larger body.

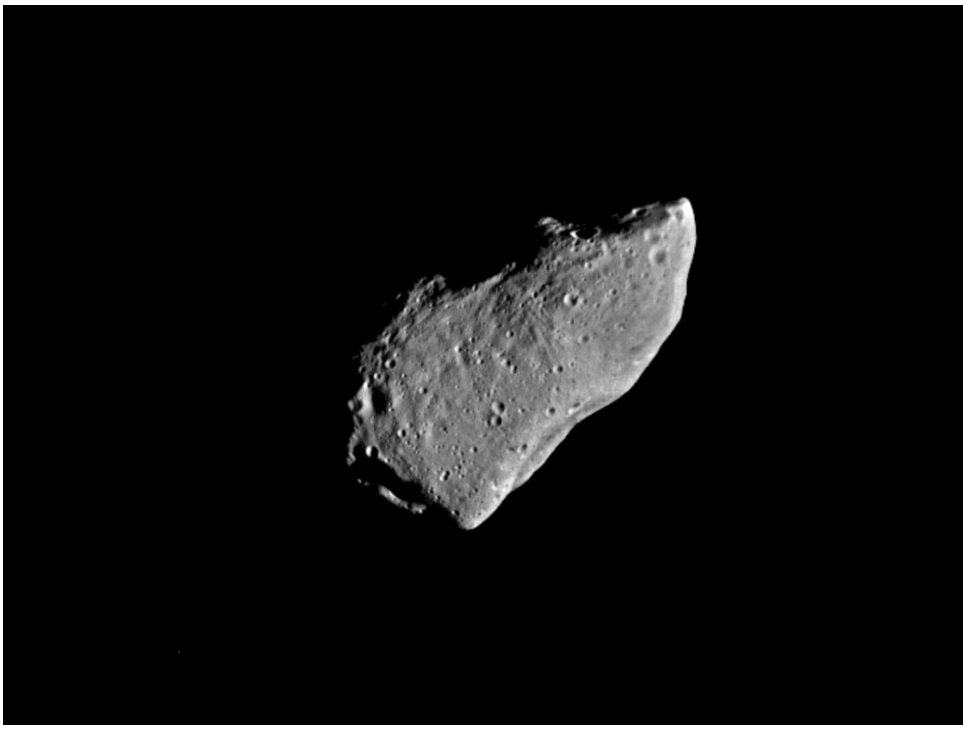

Gaspra:
• highly irregular, cratered body 18.2 x 10.5 x 8.9 km
• Irregular shape and grooves 100-300m deep suggest Gaspra to be a fragment of a larger parent body derived by catastrophic collision.
• Color variations IR/violet suggest downhill migration of a regolith.

Ida and its moon Dactyl. Ida is about 56 km long. It is a member of the Koronis family and heavily cratered. Dactyl has a size of about 1.5 km and in the image is much closer to the satellite than Ida. Density 2.6 g cm^{-3}.

Ida’s moon Dactyl

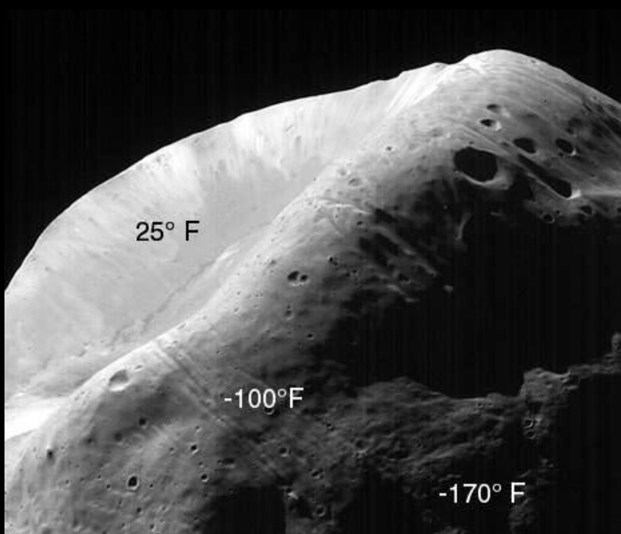

Mars’ moon Phobos Aug. 19, 1998. Size 22.5 km

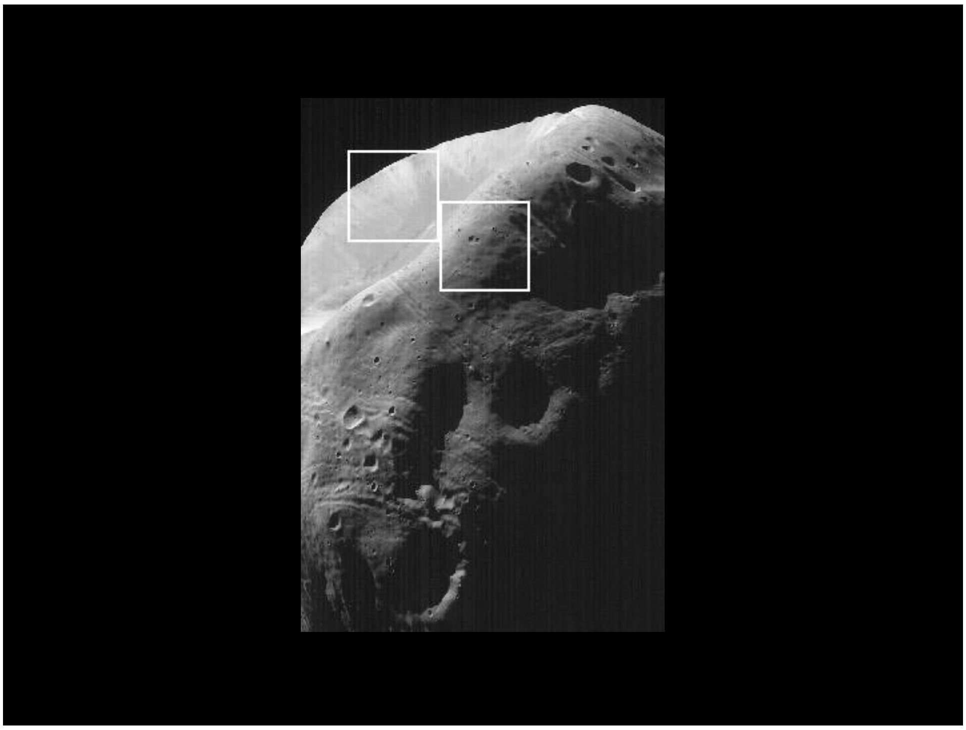

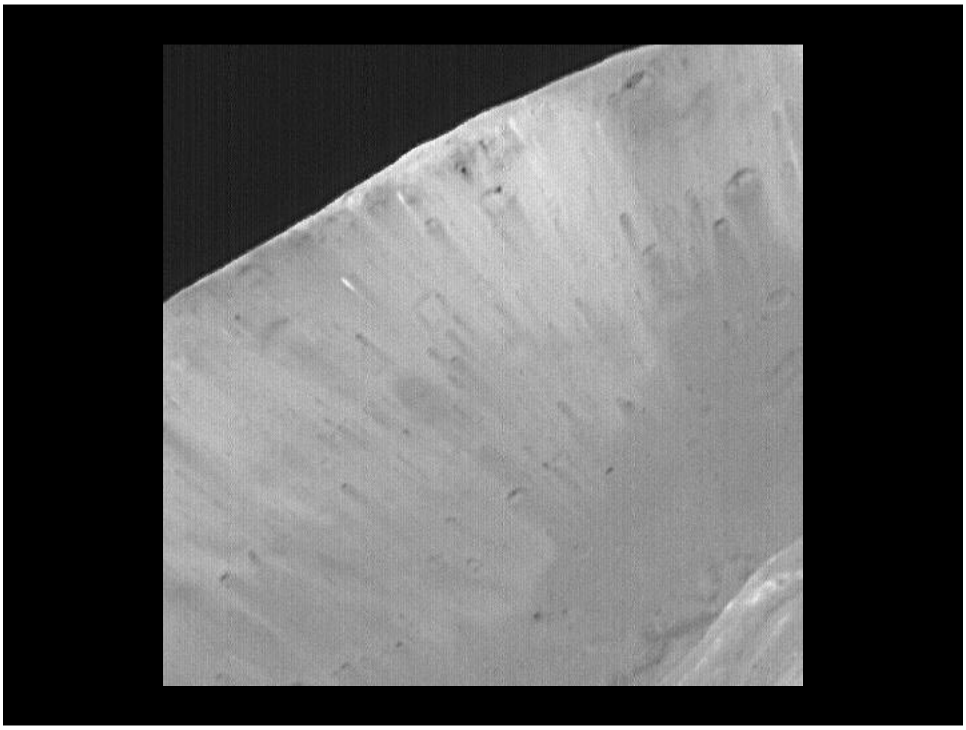

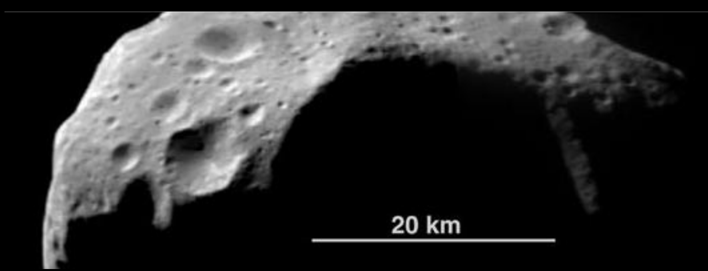

253 Mathilde, a C-type asteroid

253 Mathilde, left at $\alpha = 136^0$, right at $\alpha = 43^0$

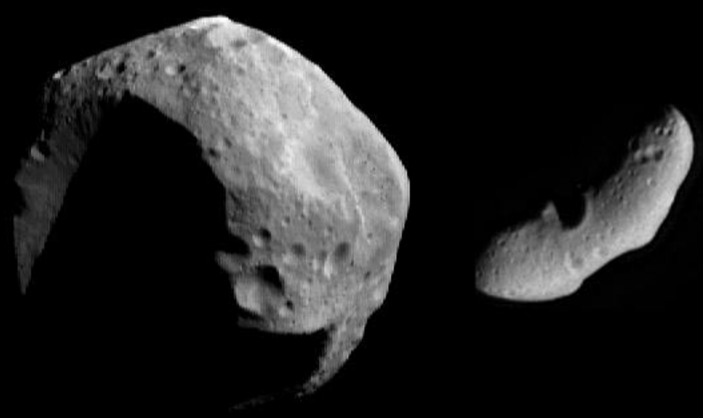

Mathilde (56 km, C-Type) and Eros (33 km, S-Type), roughly to scale

Summary of principal findings of Mathilde exploration by NEAR-Shoemaker
Cheng. A.F. “Near Earth Asteroid Rendezvous: Mission Summary”
in: Asteroids III, Bottke et al. eds. U. Arizona Space Sci. Ser. 2002, 351

- Mathilde is a classic C-type asteroid
- 50% of surface imaged during flyby. Within the 56 km diameter body on the imaged area five craters with diameters between 19 and 35km were found. 33km sized, best imaged crater is 5-6 km deep.
- Albedo 3.5-5%, similar in color to CM carbonaceous chondrites.
- Mathilde’s density is only 1.3 g cm-3. Low density either primordial, or Mathilde may be a rubble pile. There may be cavities inside Mathilde’s body.
- How can such a body withstand heavy collisions without being disrupted? The weakness of the internal structure may perhaps be its strength, as it can better dissipate the collisional energy into heat.
- No variation of optical properties depending on surface topology observed.
- No satellite found.

433 Eros 33 x 13 x 13 km, rotation period 5 hours, 16 min.

The pole axis of Eros is almost in ecliptic plane.

Plane of space probe orbit within 30° perpendicular to Sun-Eros line.

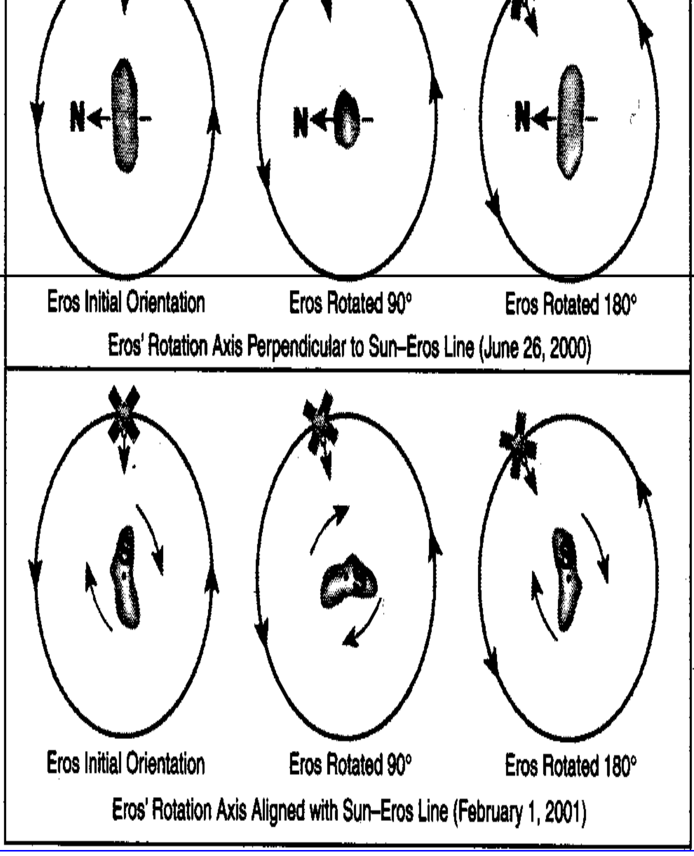

Fig. 4. *NEAR Shoemaker*'s orbital geometry at Eros in June 2000

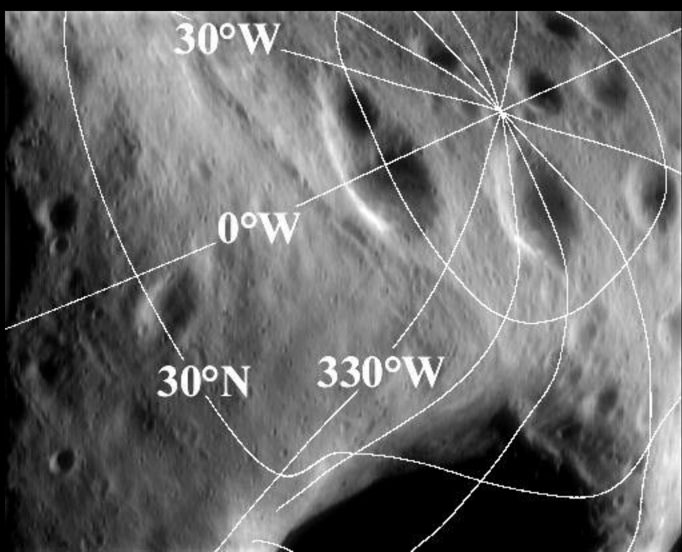

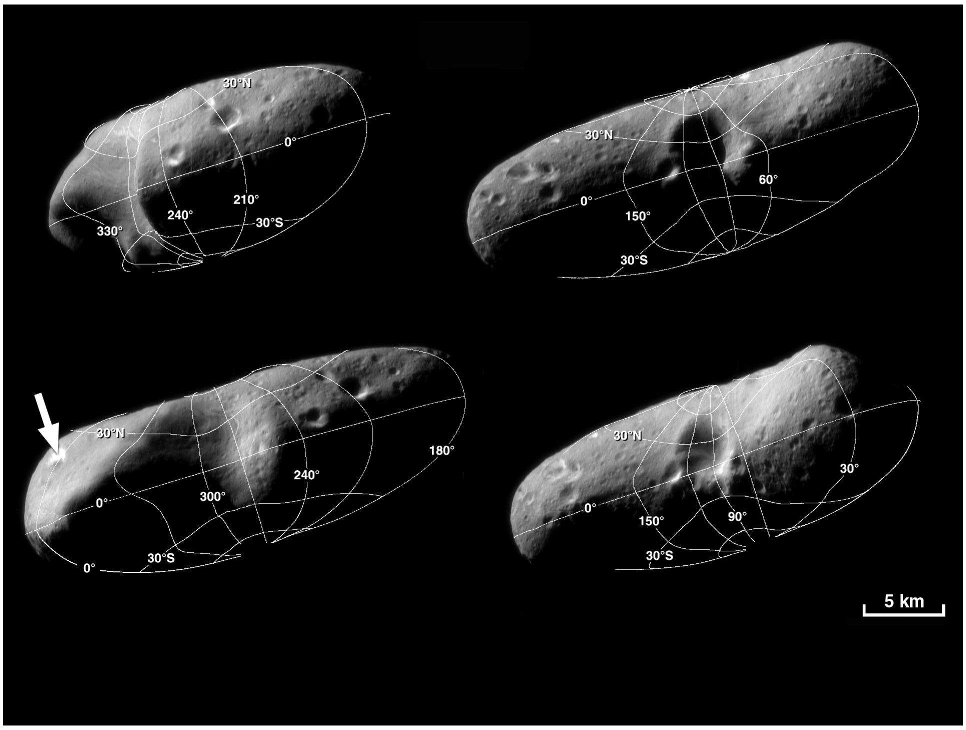
30°N
0°
210°
240°
330°
30°S
30°N
60°
0°
150°
30°S
30°N
180°
240°
300°
0°
0°
30°S
30°N
30°
0°
150°
90°
30°S
5 km

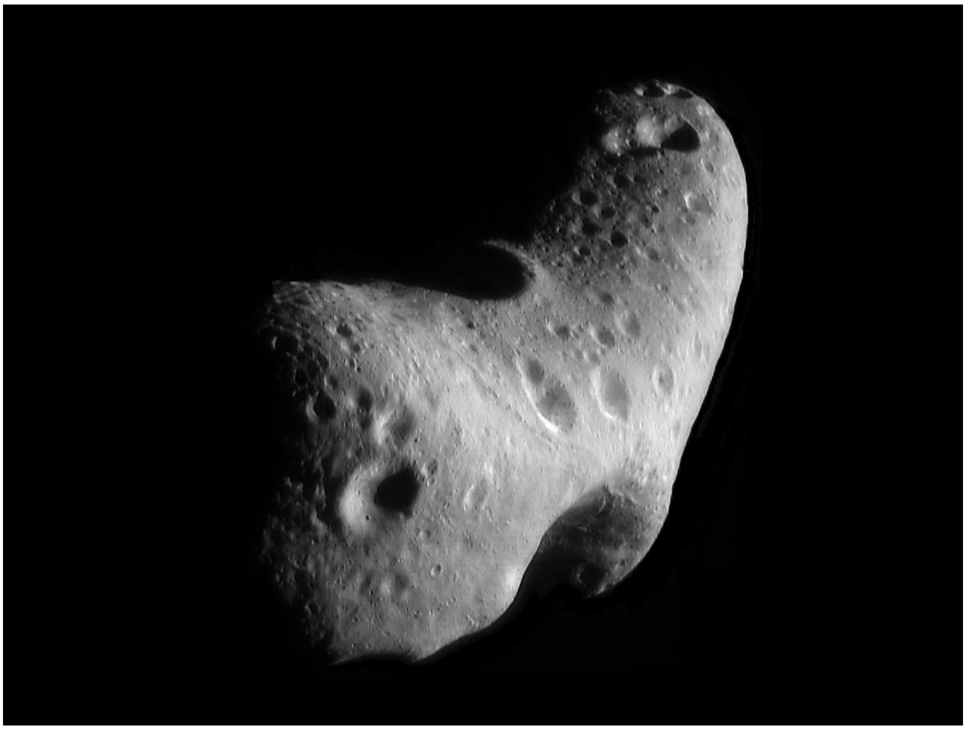

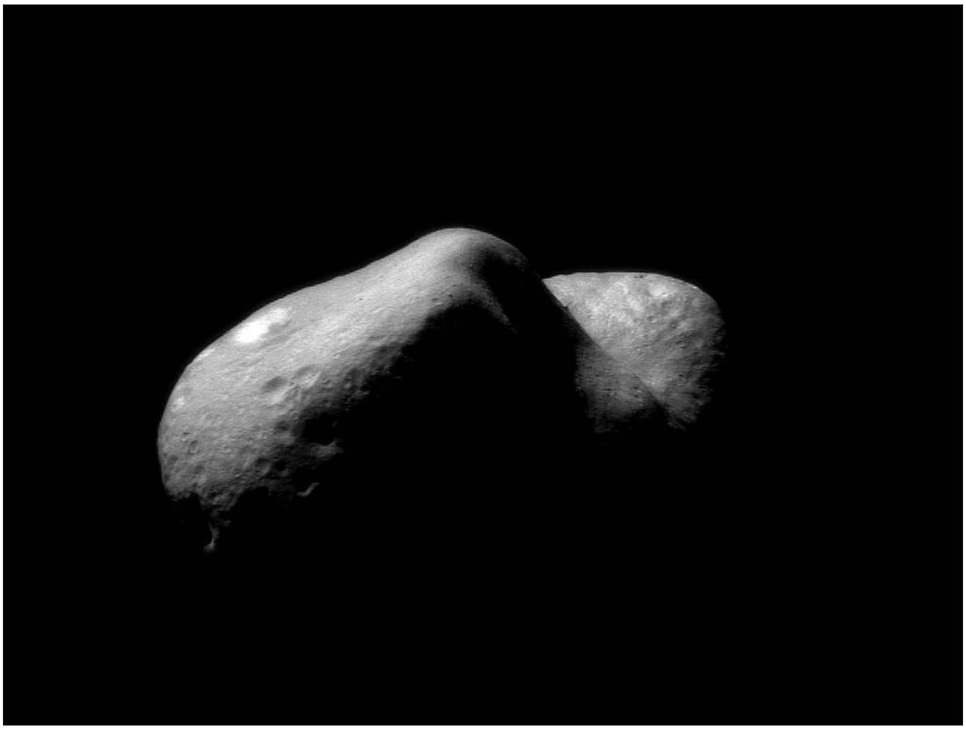

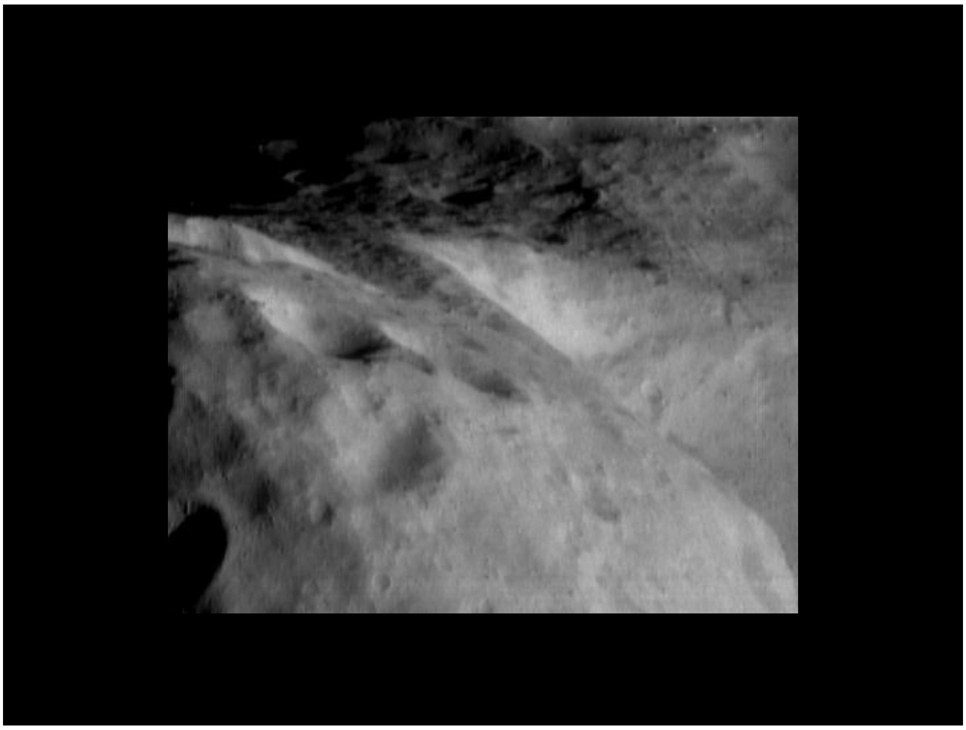

Albedo variegations

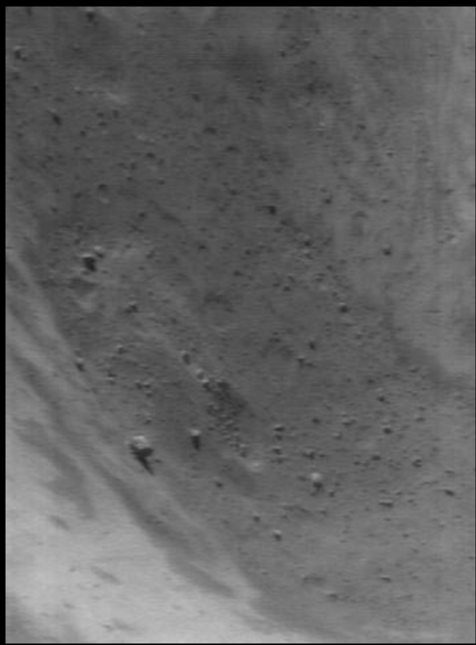

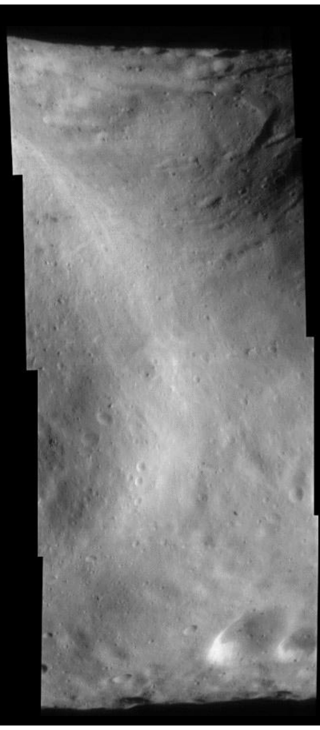

The bright curved feature is a broad topographic rise separating the saddle region from the most boulder-rich area on the asteroid .

Ridge at saddle

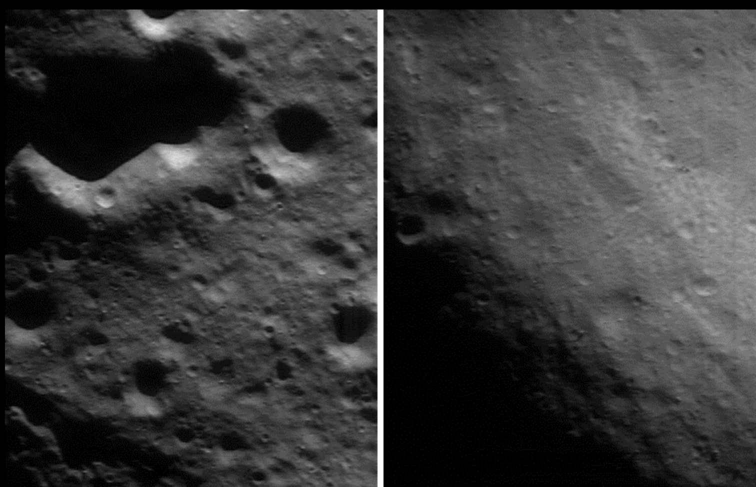

Saddle (right) has fewer crates than picture on the left side.

Another ridge at sunrise

Streaks in saddle (close-up)

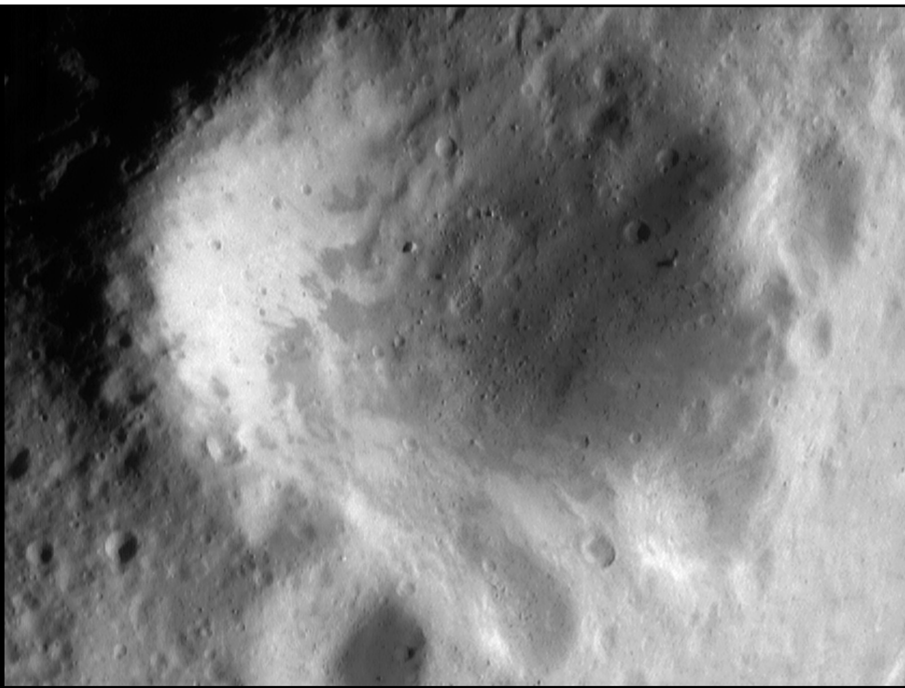

Crater Psyche

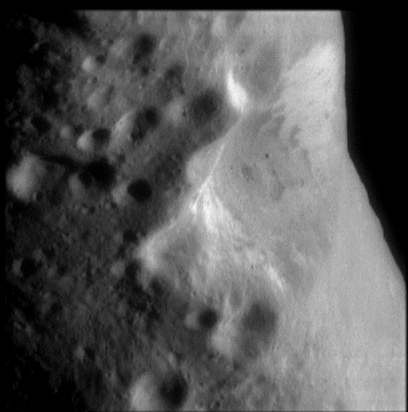

Crater Psyche, seen from other side

Steep slopes on Eros. The whole scene is 0.8 km across.

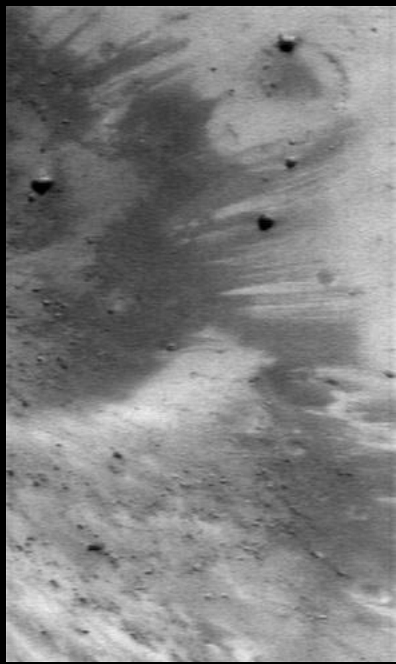

Bright crater wall.
Image is 1.2 km across.

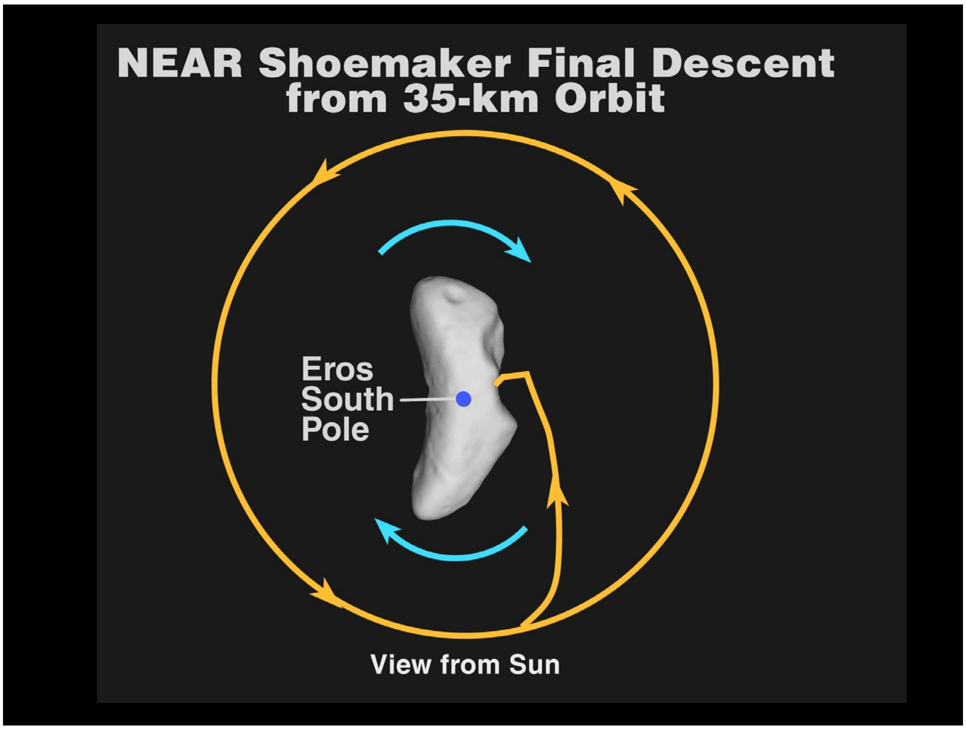
NEAR Shoemaker Final Descent
from 35-km Orbit
Eros
South
Pole
View from Sun


Near Shoemaker's landing site

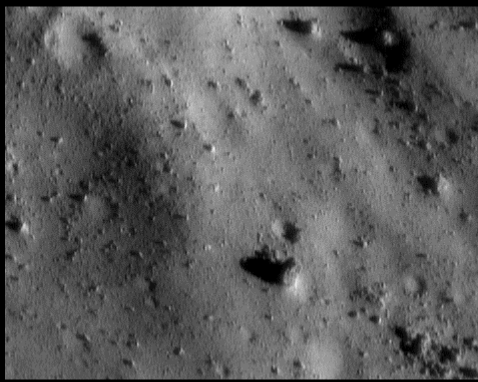

Boulder has 15m height. Note some smooth crater floors.

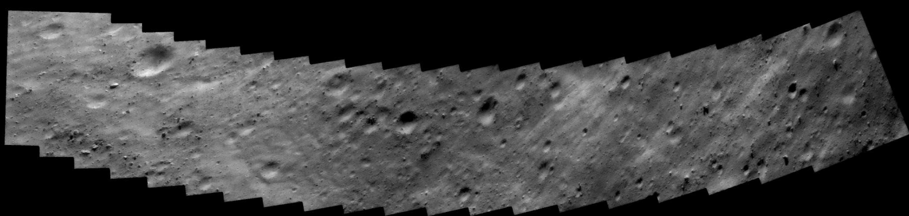

At this image the camera was only 6.4 km away from the asteroid surface. The smallest rocks are 1.4m across.

Final Eros images: Range 250 meters.

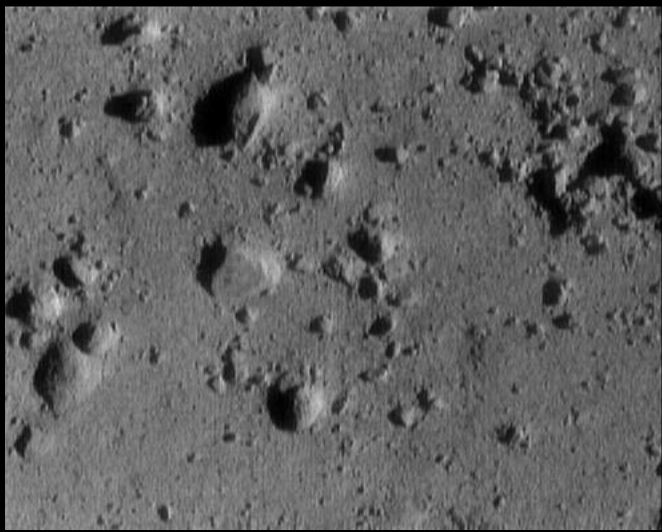

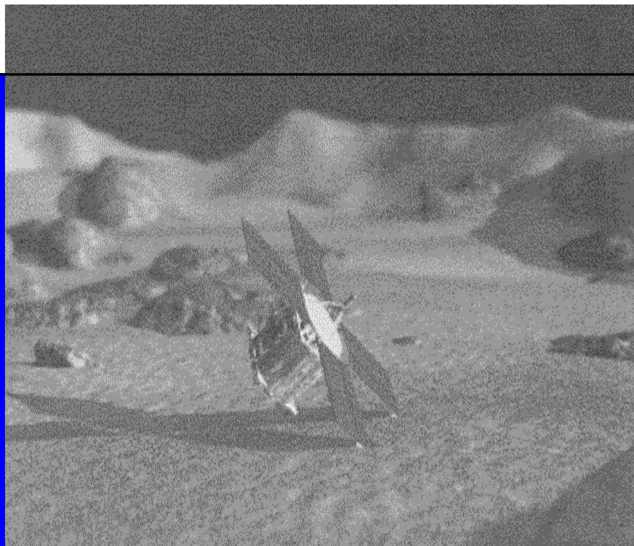

After landing on Eros the NEAR-Shoemaker spacecraft cannot produce images any more but the γ-ray spectrometer delivers high signal to noise ratio spectra of asteroid composition.

Summary of principal findings of Eros exploration by NEAR-Shoemaker
Cheng. A.F. "Near Earth Asteroid Rendezvous: Mission Summary"
in: Asteroids **III**, Bottke et al. eds. U. Arizona Space Sci. Ser. 2002, 351

- Morphology and structure: regolith tens of meters thick sometimes ponded deposits emplaced in fluidized form. Large spatial variations of large craters, dearth of small craters, high boulder densities.
- Chemical composition: consistent with ordinary chondrites, but S depleted. Perhaps Fe depleted at landing site, K chondritic.
- Faults: some evidence for faulting, homogeneous in composition.
- Overall body of Eros: largely intact but deeply fractured, most likely a fragment of a larger body, alignments of linear features suggest through-going internal structures.
- Eros precursor was primitive, but some metamorphism (partial melting) not ruled out.
- No intrinsic magnetic field found.
- No satellite found.

Global structure of asteroid 433 Eros
P. C. Thomas, L. Prockter, M. Robinson, J. Joseph, and J. Veverka:
GEOPHYSICAL RESEARCH LETTERS, VOL. **29**, NO. 10, 1408, 10.1029/2001GL014599, 2002

A global fault in Eros?

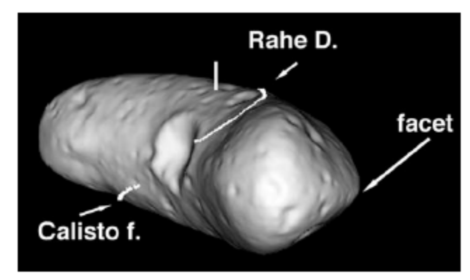

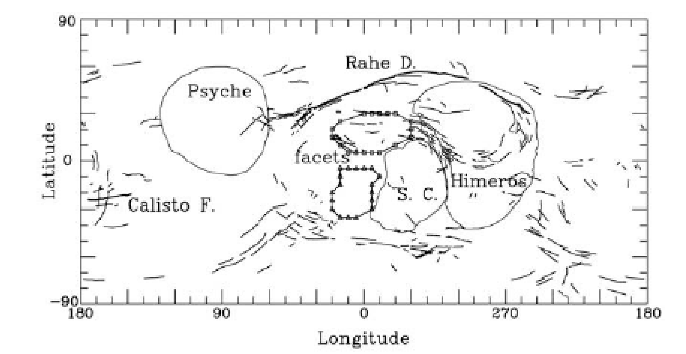

for Ida see:
Thomas et al. (1996): ICARUS **120,** 20–32

Asteroid Space weathering and regolith evolution

Beth Ellen Clark, Bruce Hapke, Carle Pieters, Daniel Britt

in: Asteroids III, Bottke et al. eds. U. Arizona Space Sci. Ser. 2002, 585

On the moon (Results from Apollo program):

Surface modification processes:

- Interplanetary dust and micrometeorite bombardment
- Solar wind implementation and sputtering
- Cosmic ray bombardment
- Meteoroid impacts

Steady state is reached when the process of pulverization is countered by agglutination and replenishment of coarser particles.

Mi

pa

red

as

mi

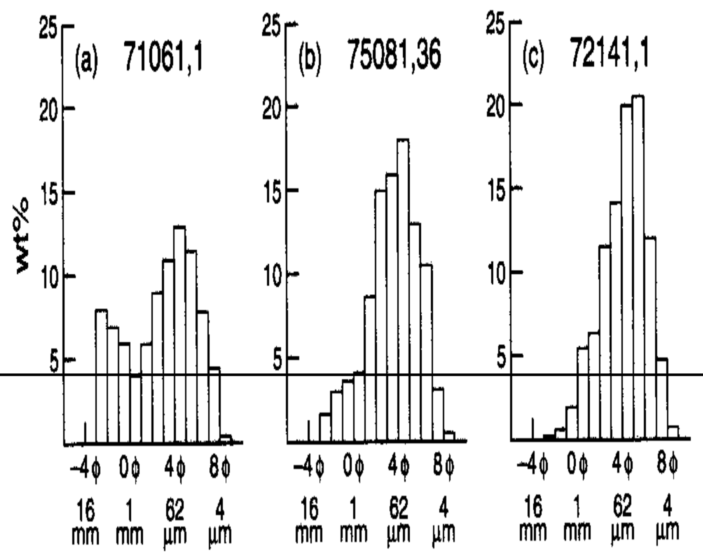

Fig. 3. Distribution of particle sizes in three Apollo 17 lunar soils in terms of mass (or volume %) of each size fraction (after *McKay et al.*, 1974): **(a)** An immature soil with a bimodal population of coarse and fine grains. **(b)** A submature soil. **(c)** A mature well-developed soil. The volumetric mean grain size of most well-developed lunar soils range from 45 to 75 µm.

Bidirectional reflectance data for size separates of lunar soil

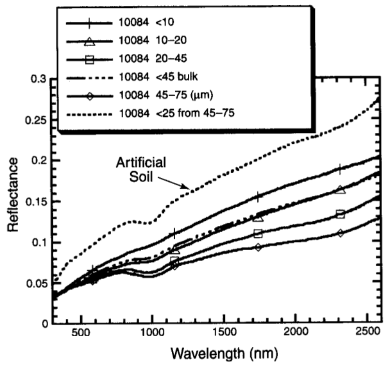

Fig. 5. Bidirectional reflectance spectra for size separates from a mature soil from Apollo 11 (10084) (data from *Taylor et al.*, 2001a; *Pieters et al.*, 1993). The bulk soil is indicated with a dot-dashed line and wet-sieved particle size separates are shown as solid lines. Note the bulk soil spectrum is dominated by the finest fractions rather than by the volumetrically dominant fractions. Note also that all size fractions of these natural soils converge at shorter wavelengths. An artificial fine fraction was prepared by grinding a subsample of the agglutinate-rich 45–75 fraction to <25 µm and is shown as a dotted line. The legend gives the size fraction in micrometers.

Transmission electron image of an anorthosite (An) grain from a mature lunar soil that exhibits a rim of Fe metal particles (SMFe)

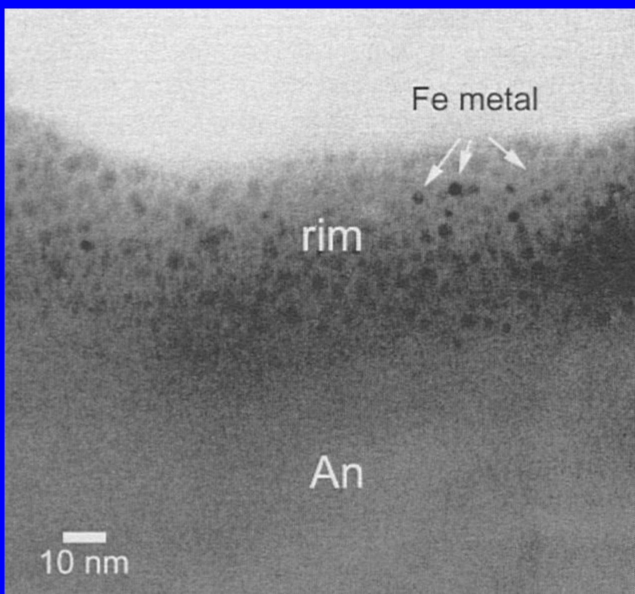

Meteorite evidence

Meteorites may be gas-rich because of implanted solar wind “gas” (He?).
• Gas rich carbonaceous chondrites do not show any spectral evidence of maturing.
• Gas rich ordinary chondrites (corresponding to S-type asteroids) do not show an increased red spectral slope. On the other hand, the slope of the meteorites is still less than the slope of the asteroids, i. e. “in lunar terms all S-type asteroids are immature”.

Reasons for immaturity of S-type asteroids:
•Lower impact velocities and solar wind flux density in asteroidal belt.
•Mineralogical differences (more silicates in the asteroids)
•More global distribution of ejecta.

Reflectance of ordinary chondrite meteorites

592 *Asteroids III*

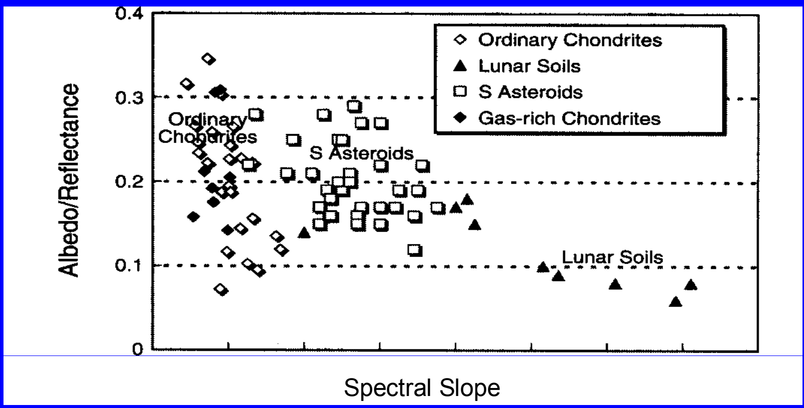

Asteroids visited by spacecraft:

951 Gaspra:
Craters on ridges tend to be slightly bluer in color than nearby surrounding terrain. Excavation of subsurface materials.
243 Ida:
Color effects on Ida similar than on the moon but magnitude of the variation is less.
253 Mathilde:
No optical alteration, because the asteroid is too dark.
433 Eros:
Clearest evidence for space weathering. High albedo contrast is accompanied by small associated spectral contrast. Different mineralogy?
On Gaspro and Ida: color contrasts high, color correlated with ejecta emplacement.
On Eros: albedo contrasts much higher than color contrasts, bright materials appear on steep crater walls.

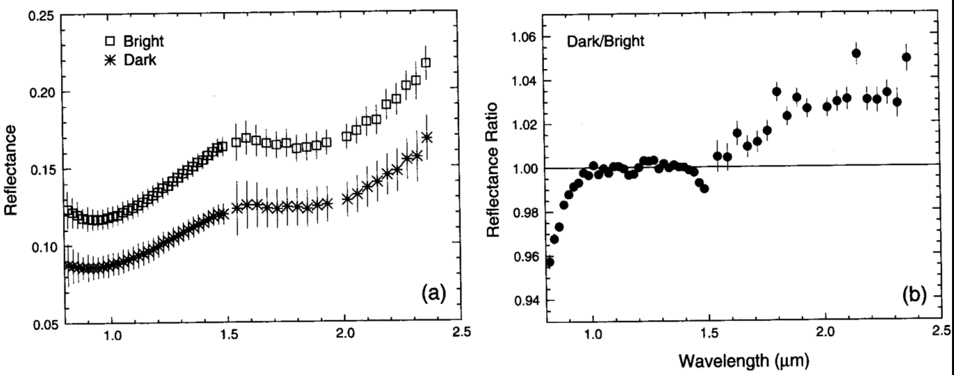

Fig. 12. **(a)** Spectra for dark and bright regions in Psyche crater. **(b)** A normalized spectral ratio of dark/bright materials. This ratio brings out the differences in spectral properties between the dark and bright materials. In general, dark materials tend to be redder from 1.5 to 2.4 µm, and slightly broader in 1-µm band depth from 0.8 to 1.0 µm (from *Clark et al.*, 2001).

Asteroids, second part.
Summary

•Reflection of light from the surface of asteroids and its relation to meteorites.
•Taxonomy of asteroids (asteroid classes) based on reflectance spectra.
•Spatial distribution of asteroid classes in the main belt.
•Thermal models of asteroids including heat transport.
•Yarkovsky effect of non-gravitational motion of small asteroidal bodies.
•Size distribution and collisional evolution of asteroids – zodiacal bands.
•Asteroid rotation
•Cratering by impacts
•Sizes and densities of asteroids
•Asteroids imaged by spacecraft: Gaspra, Ida with moon Daktyl, Matilda, Eros
•Space wethering

Origin and evolution of the asteroid belt

• Objects are differentiated, at least the larger ones.
• Some may have heavy cores and lighter mantles.
• They are remnant planetesimals which failed to accrete into a larger body.
• Mass was ejected from the asteroid belt by Jupiter.
• High temperature aggregates are found in inner regions, bound water may exist only in a few C, M, and E type asteroids.
• Gradient in mineral content with heliocentric distance
• Heating mechanism of inner asteroids by ^{26}Al?
• Large M-type asteroids may be remaining cores of disrupted asteroids.
• Metal-rich asteroids are more stable than those composed of mantle fragments.